Eur. Phys. J. D **5**, 283–289 (1999)

**THE EUROPEAN PHYSICAL JOURNAL D**

EDP Sciences


# Fragmentation of fast positive and negative $C_{60}$ ions in collisions with rare gas atoms

M.C. Larsen, P. Hvelplund[a], M.O. Larsson, and H. Shen

Institute of Physics and Astronomy, University of Aarhus, 8000 Aarhus C, Denmark

Received: 13 February 1998 / Revised: 27 October 1998 / Accepted: 29 October 1998

**Abstract.** The fragmentation of $C_{60}$ anions and cations resulting from 50 keV collisions with rare gas targets is studied. Positive ion fragment patterns are recorded, and dramatic changes in these patterns are observed as a function of target atom number. The fragment pattern dependence on the target atom size is investigated within a simple model, normally used for stopping power calculations. Fair agreement is obtained between calculated and experimental spectra. From these comparisons we conclude that the range of the screened atomic potentials, as *e.g.*, the Thomas-Fermi potential, is an essential parameter in the collisional induced fragmentation process.

**PACS.** 36.40.Wa Charged clusters – 36.90.+f Other special atoms, molecules, ions, and clusters – 61.48.+c Fullerenes and fullerene-related materials

## 1 Introduction

An analysis of collisional induced dissociation (CID) inevitably leads to questions about how energy is transferred to a molecule and how vibrational motions are energized. It has been suggested [1] that at low collision velocities ($\sim 10^7$ cm/s) the dominating dissociation mechanism is one where an atom or a group of atoms in the molecule ion suffers an elastic collision with the target atom resulting in either direct ejection or an internal vibrational excitation of the polyatomic ion.

We will try to shed some light on this suggestion by discussing CID of $C_{60}$ ions. A large number of fullerene collision studies have been reported in the past. At high collision energies fullerenes [2,3] and other types of clusters $H_{25}^+$ [4] fragment because of inelastic (electronic excitation) energy transfer in collisions with atoms or molecules. The reader is referred to the review article by Lorents [5] for further references to earlier work. In a recent publication by Ehlich *et al.* [6] fragmentation of fullerenes in low energy collisions with atomic and molecular ions was described. Measured cross-sections were compared with calculations based on a statistical RRKM theory [7] and molecular dynamics (MD) simulations [8,9], and qualitative agreement with fragmentation cross-sections were obtained for center-of-mass energies below 100 eV. Campbell *et al.* [10] have also used a statistical theory based on the maximum entropy formalism in order to explain the typical bimodal fragmentation pattern of $C_{60}$ precursors. A satisfactory complete model for CID of fullerenes is, however, still lacking. This is mainly due to the fact that MD simulations, describing the early history of the collisions, have to be combined with the long-term behaviour (decay) of excited fullerenes (statistical theories).

Here we address fragmentation in collisions between positive and negative $C_{60}$ ions and the atomic targets He, Ne and Ar at a laboratory energy of 50 keV. Only positive fragment ions are recorded after the collision and the fullerene fragment (*i.e.*, $C_n^+$ with $n > 30$) distributions are discussed and compared with model predictions.

The fragmentation model is based on calculations of elastic scattering of atoms utilizing a screened Coulomb field, as described by Lindhard *et al.* [11]. The energy transfer in collisions between the noble gas atom and each individual carbon atom is found for randomly selected impacts with the $C_{60}$ cage, and both "prompt" and delayed fragment distributions are constructed.

It is concluded that elastic collisions play a decisive role at these collision velocities and that some aspects of the collision dynamics can be understood from first principles.

## 2 Experimental

Singly charged $C_{60}$ anions – or cations – were generated in a plasma ion source and electrostatically accelerated to an energy of 50 keV. The experimental setup is described in detail in a previous publication [12]. The ions were magnetically analyzed before entering a 3 cm long differentially pumped gas cell. After exiting the target cell, the charged fast fragments scattered less than 0.5° were electrostatically separated in a 180° hemispherical analyzer with a radius of 15 cm. The analyzer voltage was swept

[a] e-mail: hvelplun@dfi.aau.dk

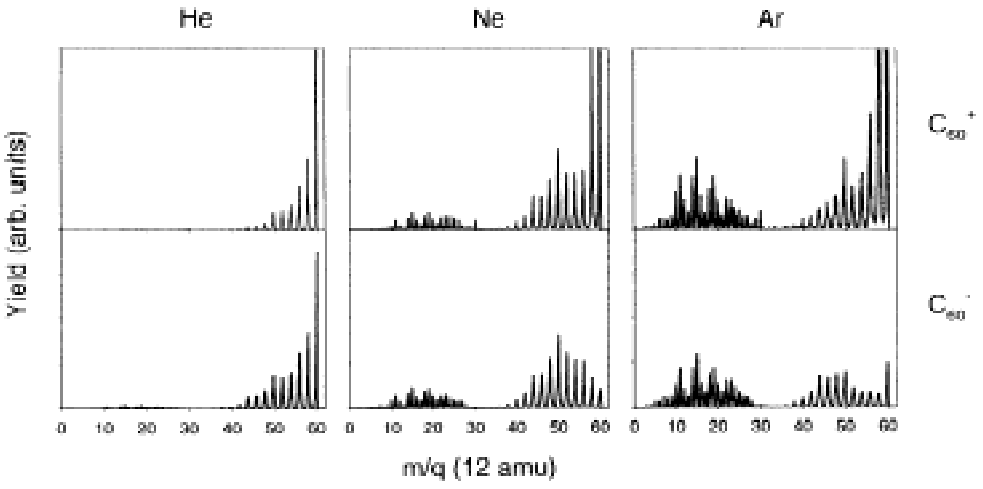


**Fig. 1.** Upper part: positive ion fragmentation spectrum obtained upon collisions of $C_{60}^+$ with He, Ne and Ar at an energy of 50 keV. Lower part: positive ion fragmentation spectrum obtained upon collisions of $C_{60}^-$ with He, Ne and Ar at an energy of 50 keV.

over the appropriate range in order to separate the fragments, and a mass spectrum was recorded since mass is proportional to energy for these high-velocity ions. Typical spectra showing positive fragment ions resulting from collisions between $C_{60}$ ions and various target gases are shown in Figure 1. The spectra were recorded for target pressures around 1 mtorr, ensuring contributions predominantly from single collisions. The distance between the ion source and the target cell is $\sim 5$ m, corresponding to a flight time of $\sim 50$ $\mu$s. We assume that ions are produced in the ion source with a broad temperature distribution and that they decay with an Arrhenius type of rate constant [13]

$$k(T) = \nu e^{-E_b/kT}, \tag{1}$$

where $T$ is the cluster temperature, $E_b$ the activation energy for the most likely decay process, and $\nu$ the preexponential factor $\sim 10^{13}$ [13,15]. If we assume that the activation energy (electron affinity) for $C_{60}^-$ is $\sim 2.7$ eV [14] and that it is $\gtrsim 7$ eV [15] for an emission of $C_2$ from $C_{60}^+$, then the maximum cluster temperature 50 $\mu$s after leaving the ion source is $\sim 1500$ K for $C_{60}^-$ and $\sim 4500$ K for $C_{60}^+$, *i.e.*, the anions will on average be much colder than the cations.

## 3 Results

Figure 1 shows typical scans of positive ion fragments obtained with anions or cations of $C_{60}$ interacting with He, Ne and Ar targets. The collision-induced dissociation (CID) spectra for anions and cations differ in two respects: $C_{60}^{++}$ ions (at $m/q = 30$), resulting from electron stripping in the collision, have only been observed in the case of the $C_{60}^+$ precursor, and the fragment peaks in the interval between $C_{52}^+$ and $C_{58}^+$ are larger for $C_{60}^+$ precursors than for $C_{60}^-$ precursors. In an earlier report [16] we showed that in the case of $C_{60}^-$ precursors also $C_n^-$ fragments with $n < 20$ are observed after collisions with various target gases, but the cross-sections are approximately 4 orders of magnitude smaller than those obtained for the $C_n^+$ fragment production.

As discussed above, the $C_{60}^-$ precursor is believed to be much colder on average than the $C_{60}^+$ precursor. Accordingly, the energy that has to be transferred in the collision before fragmentation takes place is larger for $C_{60}^-$ than for $C_{60}^+$. Also, sufficient energy for two electron strippings ($\sim 10$ eV) has to be transferred to the anion before positive fragment ions are observed. For these reasons it is plausible that large fragments will be less dominant for the $C_{60}^-$ precursors than for the $C_{60}^+$ precursors. It should also be noted that $C_{60}^{++}$ can be formed from $C_{60}^+$ by single electron stripping (ionization energy $\sim 11$ eV) [5] while three electrons with a total ionization energy of $\sim 20$ eV have to be involved for a $C_{60}^-$ precursor.

As has been noted earlier by several groups, see *e.g.* reference [6], the fragment spectra consist of a low and a high mass group, a so-called bimodal distribution. The relative intensity of the two groups changes with target gas in such a way that the small clusters dominate for heavy gases whereas the opposite is the case for light target gases. In the high mass group, only even-numbered fragments (fullerenes) are observed, in accordance with earlier observations [17]. The fragment distribution within the heavy $C_n^+$ group originating from cold $C_{60}^-$ precursors depends strongly on the target gas, as seen in Figure 1. The large difference between the He and the Ne spectra is especially striking and we will attempt to explain this difference in the following section.

## 4 Discussion

In a collision between a polyatomic ion and a target atom translational energy may be transferred either to electrons in the ion or as recoil energy to individual atoms. The competition between energy transfer to electrons and to atomic recoils has been discussed by Lindhard *et al.* [11] in connection with stopping power calculations. In descriptions of stopping power we normally talk about electronic

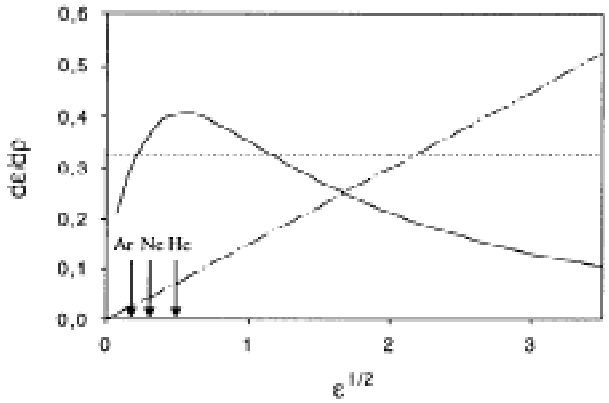


**Fig. 2.** Theoretical stopping cross-sections in $\rho - \varepsilon$ variables. The abscissa is $\varepsilon^{1/2}$, *i.e.*, proportional to projectile velocity. The solid curve is nuclear stopping computed from the Thomas-Fermi potential and the horizontal dashed line is the same computed from the screened Bohr potential. The dot-and-dash line is the electronic stopping cross-section $0.15\varepsilon^{1/2}$. The arrows indicate the $\varepsilon$ values for the different targets related to 50 keV $C_{60}$. This figure is taken from reference [19], where further details about stopping power theory can be found.

and nuclear stopping power in order to differentiate between the two energy loss mechanisms.

It turns out that the nuclear stopping is most simply described by a suitable scaling of energy and cross-section. Lindhard *et al.* [11] introduced the dimensionless quantities

$$\varepsilon = E\frac{aM_2}{Z_1Z_2e^2(M_1+M_2)} \tag{2}$$

and

$$\rho = RNM_2 4\pi a^2 \frac{M_1}{(M_1+M_2)^2} \tag{3}$$

as measures of energy and range. Here $Z_1, M_1$ and $Z_2, M_2$ are the atomic numbers and mass numbers of projectile and target atoms, respectively, and $E$ is the projectile energy. $a$=0.8853 $a_0 Z^{-1/3}$, where $Z^{2/3} = Z_1^{2/3} + Z_2^{2/3}$ and $a_0$ is the Bohr radius while $R$ is the range and $N$ is the number of atoms per unit volume. The derivative

$$\left(\frac{d\varepsilon}{d\rho}\right) = S(M_1+M_2)/4\pi a Z_1 Z_2 e^2 M_1 \tag{4}$$

is a dimensionless measure of the stopping cross-section $S = (dE/dR)(1/N)$. To a good approximation, all nuclear stopping cross-sections are then described by one curve. This is shown in Figure 2, where the solid curve was computed from a Thomas-Fermi type potential. The dashed line $(d\varepsilon/d\rho)_n = 0.327$ is computed from an $r^{-2}$ power potential [18]. The electronic stopping cross-section is nearly proportional to velocity $v$ for small $v$. This leads to an electronic stopping power

$$(d\varepsilon/d\rho) = k\varepsilon^{1/2}, \tag{5}$$

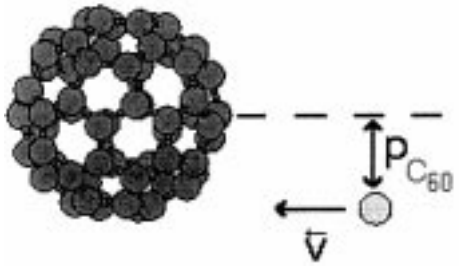


**Fig. 3.** Collision between a rare gas atom and a $C_{60}$ molecule seen from a system where $C_{60}$ is at rest. The density of carbon atoms varies strongly as a function of cage impact parameter $p_{C_{60}}$.

where $k$ is around 0.15 (*cf.* Lindhard *et al.* [19]) shown as the dot-and-dash line in Figure 2. Note from the figure that for $\varepsilon^{1/2}$ smaller than $\sim$ 2 nuclear stopping is the dominating energy loss mechanism.

Let us now turn to collisions between $C_{60}$ clusters and rare gas atoms. Let us further consider the collision in the rest frame of the $C_{60}$ cluster, Figure 3. In this system the energy of the collision partner is

$$E = \frac{M_1}{720}E_{C_{60}} \tag{6}$$

giving $E_{He} = 0.278$ keV, $E_{Ne} = 1.39$ keV and $E_{Ar} = 2.78$ keV.

The corresponding $\varepsilon^{1/2}$ values are as follows: $\varepsilon_{He}^{1/2} = 0.51$, $\varepsilon_{Ne}^{1/2} = 0.31$ and $\varepsilon_{Ar}^{1/2} = 0.17$. As seen from Figure 2, it follows that electronic "stopping" contributes less than 20% to the energy transfer to the $C_{60}$ molecules in collisions with the present target gas when its energy is 50 keV.

The total energy transfer to the fullerene cage is thus the sum of 60 binary elastic energy transfers. We assume in the following that energy transfer takes place solely in elastic binary collisions between the target atom and the individual C atoms in the cage.

Our aim is now as a function of impact parameter to calculate the energy transfer in elastic collisions with individual carbon atoms for the various target gases. Let us again turn the problem around and consider carbon as the target. For the calculations we will use the simple screened Bohr potential, which gave rise to the dashed line in Figure 2.

The interaction potential between the two atoms is assumed to be of the type

$$V(r) = \frac{Z_1Z_2}{r}u(r, Z_1, Z_2) \tag{7}$$

with

$$u(r) = \frac{k_s}{s}\left(\frac{a}{r}\right)^{s-1}, \tag{8}$$

a so-called power law potential, with the power $s$. One advantage of power law potentials is that, for several integer values of $s$, there are simple, exact scattering formulae. For the screened Bohr potential $r^{-2}$, $s = 2$ and $k_2 = 0.831$.

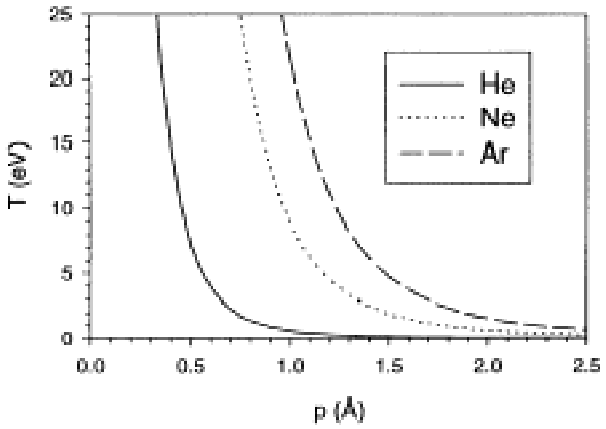


**Fig. 4.** Energy transfer $T$ in collisions between rare gas atoms and a carbon atom ($E_{\mathrm{He}} = 278$ eV, $E_{\mathrm{Ne}} = 1390$ eV, and $E_{\mathrm{Ar}} = 2778$ eV) as a function of impact parameter $p$.

For this potential the relation between the scattering angle $\theta$ in the COM system and the impact parameter $p$ can be expressed (*cf.* Lindhard *et al.* [11]) as

$$\sin\frac{\theta}{2} = \frac{\pi}{8}\,0.831\,ba\frac{1}{(p^2 + \frac{\pi}{8}0.831ba)} \tag{9}$$

where

$$b = \frac{2Z_1Z_2e^2}{M_0v^2}$$

is the so-called collision diameter and a measure of the closest approach in a head-on-collision,

$$M_0 = \frac{M_1M_2}{M_1 + M_2}$$

is the reduced mass. The energy transfer in the collision is

$$T = T_m \sin^2\frac{\theta}{2} \tag{10}$$

with

$$T_m = \frac{4M_1M_2}{(M_1 + M_2)^2}E. \tag{11}$$

The energy transfer $T$ in collisions between 278 eV He atoms, 1389 eV Ne and 2778 eV Ar atoms and free C atoms as a function of impact parameter $p$, based on equations (9, 10), is given in the table below and in Figure 4.

| $p$(Å) | $T_{\mathrm{He}}$(eV) | $T_{\mathrm{Ne}}$ (eV) | $T_{\mathrm{Ar}}$ (eV) |
|---|---|---|---|
| 0.5 | 7.2 | 91 | 198 |
| 1.0 | 0.6 | 8.9 | 21.3 |
| 1.5 | 0.0 | 1.9 | 4.7 |
| 2.0 | 0.004 | 0.6 | 1.6 |

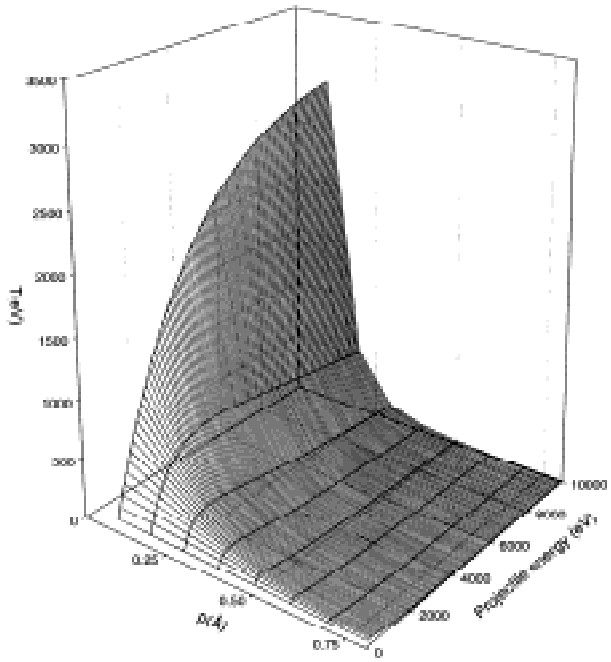

**Fig. 5.** Energy transfer $T$ in collisions between Ne and C as a function of impact parameter and projectile energy.

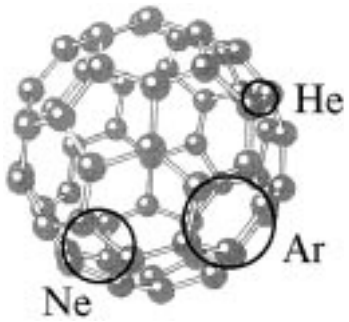


**Fig. 6.** $C_{60}$, buckminsterfullerene. The three circles indicate areas inside which knock out takes place in collisions with He, Ne and Ar.

The energy transfer as a function of impact parameter and collision energy can for any target projectile combination be calculated from equations (9–11). As an example, the energy transfer for collisions between Ne and C is shown in Figure 5. It should be noted that the energy transfer at a fixed impact parameter first increases then passes a maximum and finally decreases as a function of collision energy.

With knowledge about how to calculate the energy transfer in binary atom-atom collisions, we now address the question about fragmentation routes. We consider two, prompt and delayed fragmentation. A prompt process or a direct "knock out" is one where single C-atoms experience an energy transfer larger than $\sim 13.5$ eV, the energy required for breaking all the bonds of a single C-atom [20]. It should be noted that the "knock out" atoms can carry large amounts of energy away from the collisional interaction since we neglect interactions between these atoms

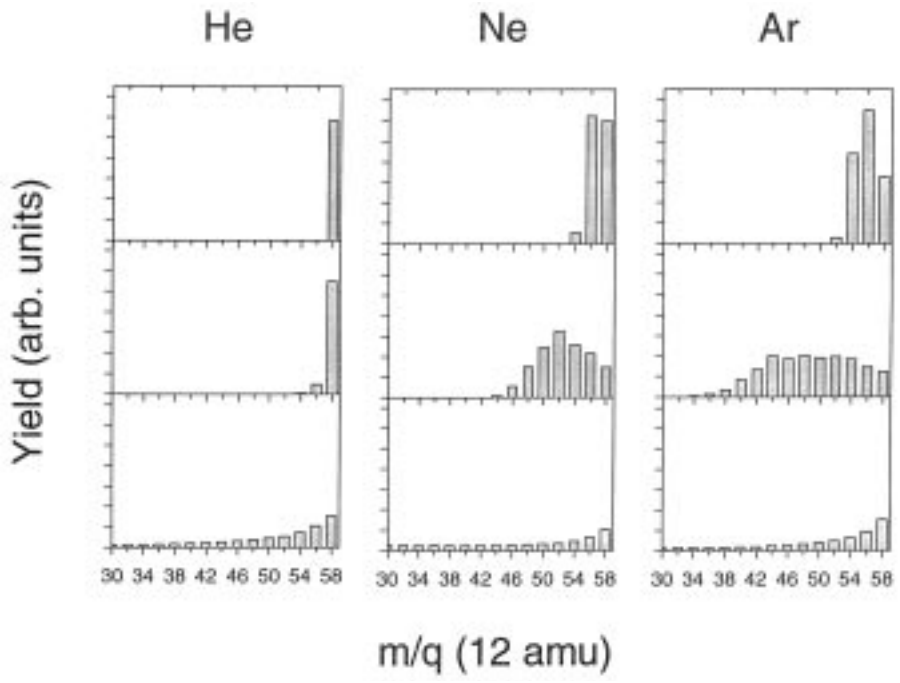


**Fig. 7.** Upper part: the calculated fragmentation spectra for the prompt knock out process only. Middle part: the calculated fragmentation spectra (prompt and delayed). Lower part: fragmentation spectra based on total energy loss calculations. The relative intensities are constructed simply by dividing the total energy loss by 7 eV. Each spectrum is based on 150 000 events. Note that the spectra in the "lower part" show fewer events since large energy transfers here result in small fragments not shown in the figure.

and the remaining "fullerene cage". Delayed fragmentation refers to the part of the energy transfer not carried away by "knock out" atoms. This part is assumed to be transferred to internal vibrational modes and released later by emission of $C_2$-dimers in "quanta" of $\sim 7$ eV per dimer. It is evident that this simplified model fails to describe the small $C_n$ fragment distribution ($n < 30$). Our aim here has been to describe the effect on the fullerene fragment distribution of the combined direct monomer knock out and subsequent evaporative $C_2$ decay. The $C_2$ evaporation model is merely a very simple approximation to a general evaporative decay process. A projection of a $C_{60}$ molecule is shown in Figure 6. On top of this projection are shown circles corresponding to areas inside which knock out would occur in collisions with He, Ne and Ar, respectively (energy transfer to individual atoms larger than 13.5 eV. It should be noted that the maximum number of knock out C atoms are $\sim 3$ for He, 7 for Ne, and 10 for Ar. The actual simulations were carried out by projecting the coordinates of the individual C-atoms in the $C_{60}$ molecule onto a plane and subsequently generating a random impact point in this plane with a $p_{C_{60}}$ (*cf.* Fig. 3) less than 8 Å. For this impact point we calculate the impact parameters and energy transfers for each quasi-free-atom in the cage. Fragmentation spectra relating to the combined prompt and delayed processes are shown in Figure 7 (middle part). When constructing these fragmentation spectra, it is further assumed that odd numbered fragments formed in a prompt process "anneal" by emitting an extra C atom before delayed $C_2$ evaporation sets in. The internal energies of the incident projectile and the resulting fullerene fragments are assumed to be equal, while an ionization energy of 10 eV is assumed to be needed for creation of positive fragments. This assumption is not strictly correct since, as argued above, positive fullerene fragments can possess more internal energy than negative ones. The calculated fragment distribution, however, is influenced only marginally by this approximation. It is clearly demonstrated how the change in impact parameters for a given energy transfer in individual rare-gas carbon-atom collisions (*cf.* Fig. 4) influences the fragment distribution. This model might serve the purpose of a simple "estimate" as to changes in fragment distribution as a function of target atomic number or impact energy.

Note that the middle part of Figure 7 represents our model calculation and that the upper and lower parts represent two extreme cases where prompt only (upper part) and delayed only (lower part) are considered. The spectra in the upper part of Figure 7 corresponds to a kind of "primitive" molecular dynamics calculation [8] where only prompt processes are considered. As discussed in reference [9], fragmentation spectra based solely on molecular dynamics calculations do not compare well with experiments. First, both odd and even fragments are formed in these simulations, and second, smaller fragments are underestimated. The lower part of Figure 7 reflects the situation where the full energy lost by the projectile is transferred to the cage *via* C–C interactions and hence corresponds to the other extreme where the low mass C fragments are expelled from the cage with close to zero kinetic energy.

The calculated mass spectra (Fig. 7 middle part) are compared with the experimental ones ($C_{60}^-$ resulting in positive fragments in rare gas collisions) in Figure 8. The model calculations are seen to reproduce the qualitative features of the Ne and Ar spectra quite well. They reproduce the peaked distribution for the Ne collisions, and the intensity plateau for the Ar collisions. The He spectrum is not reproduced nearly as well. In fact, the measurements for this case are in better accordance with the

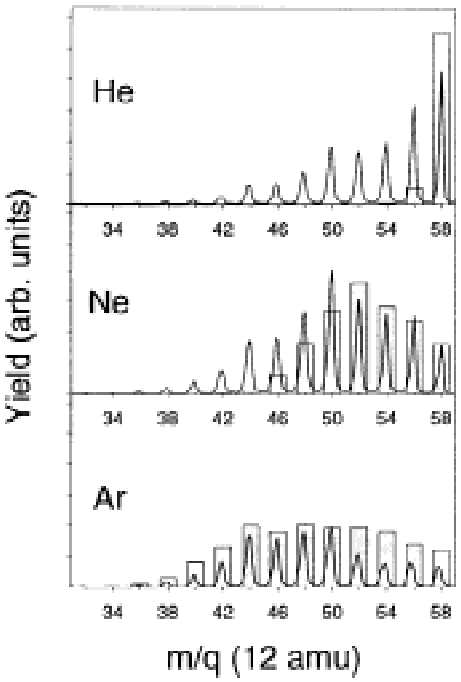


**Fig. 8.** Comparison of the calculated (bars) fragmentation spectra (prompt and delayed) with experimental spectra (continuous line).

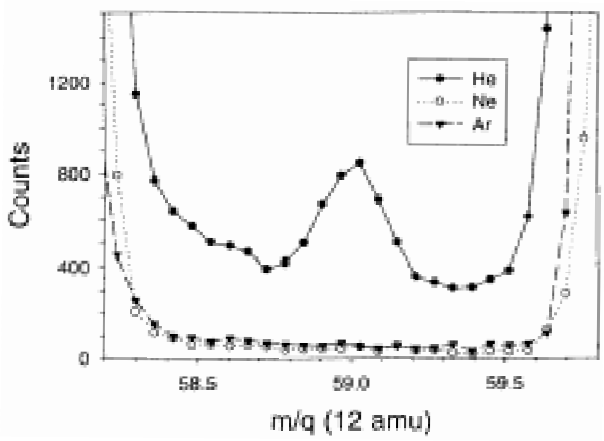


**Fig. 9.** Positive ion fragmentation spectra for 50 keV $C_{60}^-$ in collisions with He, Ne, and Ar. The spectra emphasizes the fragment size $C_{59}^+$ but is a slice of the spectra shown in Figure 1 (lower part).

calculation based on a pure evaporative model (Fig. 7 lower part). This observation makes, in fact, good sense. As can be seen from Figure 5, low energy recoils have a much smaller chance to "escape" the cage without losing energy than the high energy ones. A scenario where the total projectile energy loss to the carbon cage is transferred into internal energy seems to apply for collisions with He. This energy is then in our model used for $C_2$ evaporation. For the Ne and Ar collisions part of the "knock outs" are "escaping" with large kinetic energy and our model calculation, which neglects interaction between "knock outs" and the remaining cage atoms, applies better for these gases.

From the discussion above we have learned that the pronounced differences in fragmentation patterns, observed for relatively cold $C_{60}^-$ ions (lower part of Fig. 1), are governed by an interplay between the energy transfer in binary atom-atom collisions and by the ability of the cage to redistribute this energy in a statistical way. The often-used phrase that the fragmentation patterns are different because of differences in the center-of-mass energy are, as can be seen, at the best meaningless and can lead to false conclusions. Model calculations on fragmentation of $C_{60}^+$ have not been attempted since the initial state of positive fullerene projectiles is less well defined than that for negative fullerenes. From a comparison of the two fragmentation spectra for, say, the Ar target, it has been observed that $C_{58}^+$, $C_{56}^+$ and $C_{54}^+$ peaks are more predominant for $C_{60}^+$ projectiles than for $C_{60}^-$ projectiles. Such a difference would be expected since distant collisions, which lead to delayed fragmentation only, become relatively more important for "hot" projectiles.

A careful examination of the $C_{60}^-$+ He fragmentation spectrum reveals a small peak corresponding to $C_{59}^+$. As shown in Figure 9, this peak only appears in collisions with He. We take this observation as extra evidence for the importance of a direct knock-out process. Simulations carried out using the model described above shows that a He atom at our energy can penetrate the $C_{60}$ cage without inducing any fragmentation ($\sim$ 7%). When Ne or Ar hits the cage, fragmentation will always occur at our collision energy. Following this line of thought, it is easy to visualize an event where the He atom knocks out a single C-atom but otherwise transfers very little energy to the cage. This process may be dubbed "needle fragmentation". It has earlier been observed [21] that $C_{59}^+$, unlike other odd-numbered fullerenes, exists for a time long enough to make detection possible. The structure and stability of this so-called "pseudo-fullerene" have been addressed in theoretical studies [22], where it was found that the most stable structure includes heptagons and octagons. The stability of $C_{59}$ was found to be relatively high. It is also interesting to note that $C_{59}^+$ is not detected when $C_{60}^+$ is colliding with He at the same energy. This difference is ascribed to the difference in internal energy for the positive and negative $C_{60}$ ions. For fragmentation of $C_{60}^+$, ejection of a single C-atom will lead to "annealing" of the $C_{59}^+$ cage, resulting in $C_{58}^+$.

## 5 Conclusion

We have studied the fragmentation patterns of $C_{60}^-$ and $C_{60}^+$ in collisions with rare gases. We found that the positive ion fragment patterns depend strongly on the charge state of the precursor. This effect is ascribed to large differences in temperature for the two kinds of $C_{60}$ beams. The larger clusters show very different fragmentation patterns for different target gases. This observation is explained as a result of differences in energy transfer as a function

of impact parameter in atom-atom collisions. It is concluded that collisional fragmentation is partly a result of direct "knock-out" processes and partly delayed evaporation, most probably dominated by $C_2$ emission.

The existence of a $C_{59}^+$ peak in the fragment spectrum, resulting from the process $C_{60}^- + He \rightarrow C_{59}^+$, is taken as further evidence for a direct "knock-out" mechanism.

One of the authors (PH) would like to take this opportunity to thank Jens Lindhard for many stimulating discussions about fragmentation of $C_{60}$. Many of the problems encountered in this article have been discussed with him during the last few years. The present work has been supported by the Danish National Research Foundation through the Aarhus Center for Atomic Physics (ACAP).

## References

1. J. Durup, in *Recent Developments in Mass Spectrometry*, edited by K. Ogata, T. Hayakawa (University Park Press, Baltimore, MA, 1970), p. 921.
2. T. LeBrun, H.G. Berry, S. Cheng, R.W. Dunford, H. Esbensen, D.S. Gemmell, E.P. Kanter, Phys. Rev. Lett. **72**, 3965 (1994).
3. A. Reinköster, U. Werner, H.O. Lutz, Europhys. Lett. **43**, 653 (1998).
4. B. Farizon, M. Farizon, M.J. Gaillard, R. Genre, S. Louc, J. Martin, J.P. Buchet, M. Carré, G. Senn, P. Scheier, T.D. Märk, Int. J. Mass Spectro. Ion Proc. **164**, 225 (1997).
5. D.C. Lorents, Comm. At. Mol. Phys. **33**, 125 (1997).
6. R. Ehlich, M. Westerburg, E.E.B. Campbell, J. Chem. Phys. **104**, 1900 (1996).
7. M. Foltin, M. Lezius, P. Scheier, T.D. Märk, J. Chem. Phys. **98**, 9624 (1993).
8. R. Ehlich, E.E.B. Campbell, O. Knospe, R. Schmidt, Z. Phys. D **28**, 153 (1993).
9. J.A. Spirko, A.P. Hickman, Phys. Rev. A **57**, 3674 (1998).
10. E.E.B. Campbell, T. Raz, R.D. Levine, Chem. Phys. Lett. **253**, 261 (1996).
11. J. Lindhard, V. Nielsen, M. Scharff, Mat. Fys. Medd. Dan. Vid. Selsk. **36** (1968).
12. H. Shen, P. Hvelplund, D. Mathur, A. Bárány, H. Cederquist, N. Selberg, D.C. Lorents, Phys. Rev. A **52**, 3847 (1995).
13. J.U. Andersen, C. Brink, P. Hvelplund, M.O. Larsson, B. Bech Nielsen, H. Shen, Phys. Rev. Lett. **77**, 399 (1996).
14. L.-S. Wang, J. Conceicao, C. Jin, R.E. Smalley, Chem. Phys. Lett. **182**, 5 (1991); C. Brink, L.H. Andersen, P. Hvelplund, D. Mathur, J.D. Voldstad, *ibid.* **233**, 52 (1995).
15. R. Wörgötter, B. Dünser, P. Scheier, T.D. Märk, M. Foltin, C.E. Klots, J. Laskin, C. Lifshitz, J. Chem. Phys. **104**, 1225 (1996).
16. D. Mathur, C. Brink, P. Hvelplund, N. Jensen, D.H. Yu, Rapid Comm. Mass Spect. **9**, 114 (1995).
17. R.J. Doyle, M.M. Ross, J. Phys. Chem. **95**, 4954 (1991).
18. N. Bohr, Mat. Fys. Medd. Dan. Vid. Selsk. **18** (1948).
19. J. Lindhard, V. Nielsen, M. Scharff, P.V. Thomsen, Mat. Fys. Medd. Dan. Vid. Selsk. **33** (1963).
20. E.S. Parilis, Nucl. Instr. Meth. Phys. Res. B **88**, 21 (1994).
21. T. Weiske, D.K. Böhme, J. Hrušák, W. Krätschmer, H. Schwarz, Angew. Chem. Int. Ed. Engl. **30**, 884 (1991).
22. M.-L. Sun, Z. Slanina, S.-L. Lee, Fulleren Sci. Techn. **3**, 627 (1995).